

Two-dimensional index profiling of fibers and waveguides

Norman H. Fontaine and Matt Young

We have constructed a two-dimensional refracted-ray scanner that can resolve index-of-refraction increments of approximately 4×10^{-5} . This resolution is an order of magnitude finer than the uncertainty of the measurement. The scanner can be adapted to evaluate either fibers or planar waveguides. The two-dimensional scan and the high precision allow visualization of features, such as deposition layers, that are difficult if not impossible to see in conventional one-dimensional scans.

OCIS codes: 060.0060, 130.0130, 060.2300, 060.2430.

1. Introduction

We have developed an apparatus for measuring index profiles in two dimensions. The profiler uses the refracted-ray method,^{1,2} or refracted near-field scanning, and can be fairly easily adapted to measurements of optical fibers or integrated-optical waveguides. The index resolution is of the order of 4×10^{-5} and is so fine that the deposition layers can be seen in a two-dimensional (2-D) plot of a multi-mode fiber. Spatially, the instrument is approximately diffraction limited.

Many new components, such as waveguide lasers, require precise control over the mode field and the phase of the light that propagates into and out of them. The mode field and the phase depend entirely on the index profile. Therefore the research, development, and production of these fibers and waveguides can be enhanced by precise measurements of the index profiles, particularly with low uncertainty and high spatial resolution. The refracted-ray method is the reference method of the Telecommunications Industry Association.³

One way to calibrate a refracted-ray scanner is to relate the measured intensity of the refracted light to the index of refraction at two or more reference points.¹ The standard uncertainty of an index profile can be only as good as the standard uncertainty of

the indices at those reference points. In contrast, the resolution of the index profile depends mainly on noise and may be substantially less than the standard uncertainty of the measurement. That is, the detail with which we can observe real index features is independent of the calibration but rather depends solely on the resolution of the measurement. Resolution depends primarily on laser fluctuations, so we can improve the resolution of the measurement by improving the stability of the laser and the photodetector, regardless of whether we can reduce the standard uncertainty introduced by the calibration. This statement presupposes that the resolution is not degraded by inhomogeneities in the specimen itself or in the coverslip, or by contamination on the surfaces of either.

2. Theory

Let us first estimate the magnitude of the uncertainties of the index of refraction of typical materials that may be used as references. The index of the cladding of silica waveguides can vary by approximately 7×10^{-4} , depending on the method of manufacture.⁴ The uncertainty of the increments of the index of a fiber that is designed specifically for reference has been reported as 5×10^{-5} .⁵ Thermal variations of the index of these solid materials are normally less than a few times 10^{-5} K and can usually be ignored. Thus for a well-known solid such as silica, the uncertainty of the reference index lies between 5×10^{-5} and 7×10^{-4} .

Index-matching fluids display typical batch-to-batch variations between 2×10^{-4} and 5×10^{-4} and thermal coefficients of approximately $-4 \times 10^{-4}/\text{K}$.⁶ If we assume that the temperature of the specimen can be measured and controlled within approximately 1 K during data acquisition and calibration, then the standard uncertainty of the index of a typ-

When this research was performed, the authors were with the Optoelectronics Division, National Institute of Standards and Technology, 325 Broadway, Boulder, Colorado 80303. N. Fontaine is now with PK Technology, 9405 S.W. Gemini Drive, Beaverton, Oregon 97005. M. Young is with the Department of Physics, Colorado School of Mines, 1500 Illinois Street, Golden, Colorado 80401. His e-mail address is myoung@mines.edu.

Received 14 April 1999; revised manuscript received 21 July 1999.

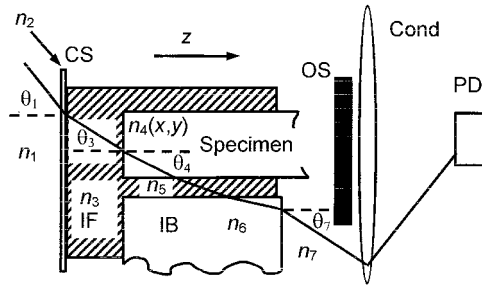


Fig. 1. Ray trace of the light propagating in a refracted-ray scanner configured for profiling a planar waveguide. The basic components are the photodetector (PD), condensing lens (Cond), opaque stop (OS), index-matching block (IB) with index n_6 , specimen with index $n_4(x, y)$, index-matching fluid (IF) with index n_3 , and coverslip (CS) with index n_2 . The light refracts through two corners in medium 4 and medium 6.

ical fluid is between 6×10^{-4} and 9×10^{-4} . To place these numbers in the context of an index profile measurement, an uncertainty in the index of a reference point in a fluid of 9×10^{-4} is equivalent to 17% of the core-cladding index difference Δn of a typical single-mode fiber used by the telecommunications industry ($\Delta n \approx 5 \times 10^{-3}$). An uncertainty in a solid reference material of 2×10^{-4} is equivalent to 3.8% of the index difference of the same single-mode fiber. Thus the index of the fluid is the dominant source of uncertainty.

A. Converting the Measured Intensity to the Index of Refraction

When a wave front passes through an abrupt change of the index of refraction, the component of the wave vector perpendicular to the direction of index change is conserved. In Fig. 1 we define the angle of refraction relative to the z axis. A wave vector refracts through a horizontal index change between adjacent layers i and $i - 1$ according to

$$n_i \sin(\theta_i) = n_{i-1} \sin(\theta_{i-1}). \quad (1)$$

The wave vector refracts through a vertical index change according to

$$n_i \cos(\theta_i) = n_{i-1} \cos(\theta_{i-1}). \quad (2)$$

In refracted-ray scanning, both sides of an interface separating distinct regions must be homogeneous, with the exception of the endface of the specimen (medium 4). When the wave vector refracts through a 90° corner of the specimen and a 90° corner of a block (medium 6), the index of refraction $n_4(x, y)$ at the point (x, y) on the specimen is related to angle of incidence θ_3 and the final angle of refraction θ_7 by¹

$$n_4^2(x, y) = n_6^2 + n_3^2 \sin^2(\theta_3) - n_7^2 \sin^2(\theta_7). \quad (3)$$

(This relation also holds if the block is removed and the immersion fluid forms the 90° corner. Then n_6 is equal to n_3 .) When the indices of refraction n_6 and

$n_4(x, y)$ differ by a small increment $\delta n_4(x, y)$, we can write

$$\begin{aligned} n_4^2(x, y) &= [n_6 + \delta n_4(x, y)]^2 \\ &\approx n_6^2 + 2n_6 \delta n_4(x, y). \end{aligned} \quad (4)$$

The numerical aperture of the light that exits a filled or overfilled objective lens is conserved when the light refracts through an interface between two homogeneous media. Thus the numerical aperture (NA) is

$$\text{NA}_{\text{obj}} \equiv n_1 \sin(\theta_{1,\text{max}}) = n_3 \sin(\theta_{3,\text{max}}), \quad (5)$$

where $\theta_{i,\text{max}}$ is the vertex angle i of the focused cone of light in medium i .

In the refracted-ray method, a stop must be centered on the optical axis to block leaky rays and guided light within an inner cone of vertex angle θ_{stop} . The total power $P(\theta_7)$ of refracted light transmitted past the stop by a Lambertian source is related to the angle of refraction θ_7 by

$$P(\theta_7) = B[n_7^2 \sin^2(\theta_7) - \text{NA}_{\text{stop}}^2], \quad (6)$$

where B is a constant of proportionality. Substituting Eqs. (4)–(6) into Eq. (3) yields

$$\delta n_4(x, y) \approx \frac{\text{NA}_{\text{obj}}^2 - \text{NA}_{\text{stop}}^2}{2n_6} - \frac{P(\theta_7)}{2n_6 B}. \quad (7)$$

When a Lambertian source is used, the power transmitted past the stop is nearly linearly related to the index difference $\delta n_4(x, y)$. Even if the source is a point source, not a Lambertian source, the power transmitted past the stop is a nearly linear function of $\delta n_4(x, y)$.¹ In addition, provided that the beam at the focal point is diffraction limited, the spatial resolution of a refracted-ray scan is diffraction limited when the numerical aperture of the stop is $\text{NA}_{\text{stop}} \approx 0.7 \text{NA}_{\text{obj}}$.

When the refracted light is completely blocked by the stop, the measured intensity $P(\theta_7)$ is 0. Substitution of $\text{NA}_{\text{stop}} = 0.7 \text{NA}_{\text{obj}}$ and $P(\theta_7) = 0$ into approximation (7) shows that the maximum index in the guiding channel that can be measured by refracted-ray scanning with diffraction-limited spatial resolution is $\max[\delta n_4(x, y)] = 0.51 \text{NA}_{\text{obj}}/2n_6$. For example, assume that we use an objective with a numerical aperture $\text{NA}_{\text{obj}} = 0.65$ and an index-matching block of fused silica ($n_6 = 1.4570$). Approximation (7) limits the measurable index difference to roughly $\max[\delta n_4(x, y)] = 0.074$ while maintaining diffraction-limited spatial resolution.

B. Aligning the Specimen and Focusing the Objective

The index profiler must be designed so it is easy to align and to orient the endface of the specimen parallel to the focal plane of the objective. The goal is to make it easy to obtain diffraction-limited performance across the entire length or area of the mea-

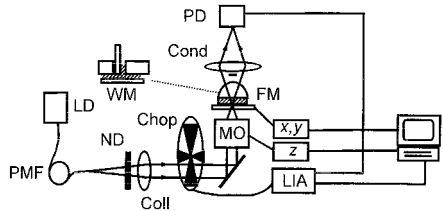


Fig. 2. Schematic of the apparatus used in this research. The components are the laser diode (LD), polarization-maintaining fiber (PMF), neutral density filter (ND), collimating lens (Coll), chopper wheel (Chop), microscope objective (MO) controlled by a z-axis stepping motor (z), scanning platform controlled by x, y-axis stepping motors (x, y), condensing lens (Cond), photodiode (PD), and lock-in amplifier (LIA). The fiber mount (FM) and the waveguide mount (WM) are interchangeable, as indicated by the dotted line.

surement. When light of wavelength λ is focused by an objective, the depth of focus d is approximately

$$d = \lambda \sqrt{1 - \text{NA}_{\text{obj}}^2} / 2 \text{NA}_{\text{obj}}^2 \quad (8)$$

according to Shillaber's equation.⁷ Here the depth of focus is the distance between the focal plane and the plane where the image loses sharp focus. We must focus the beam onto the end of the fiber with a precision much less than d . In addition, as the end of the fiber is scanned across the focal point, it must remain within d of the focal plane. Otherwise, diffraction-limited performance is lost, and artifacts appear in the index profile. Hence the endface of the specimen must be parallel to the focal plane of the objective. For example, if we want to scan $7.5 \mu\text{m}$ on either side of a fiber (with a cladding radius of $62.5 \mu\text{m}$), we need to remain within focus over $70 \mu\text{m}$ on each side of the fiber axis. The angular misalignment tolerance between the normal to the specimen and the axis of the beam must therefore be no more than $\tan^{-1}(0.6/70) \approx 0.5^\circ$, presuming that the instrument is well focused at the center of the fiber.

3. Apparatus and Technique

The source was a Peltier-cooled, temperature-controlled laser diode that operated at $\lambda = 635 \text{ nm}$ (see Fig. 2). The laser had periodic intensity fluctuations with a maximum relative deviation of 0.22% about the mean and a relative standard deviation of approximately 0.1% (see Fig. 3). Lasers that are not temperature controlled will typically display frequent mode hopping and random intensity fluctuations of the order of 0.5% and greater. We chose a laser diode over a helium-neon laser because the typical helium-neon laser displays long-term drifts of approximately 2%, or an order of magnitude more than the shorter-term fluctuations of the laser diode.

The output of the laser was coupled to a 1-m patch-cord of single-mode polarization-maintaining (PM) fiber. We did not look carefully at the polarization dependence of the system but maintained the direction of the electric vector perpendicular to the scanning direction. The light output in the vicinity of the

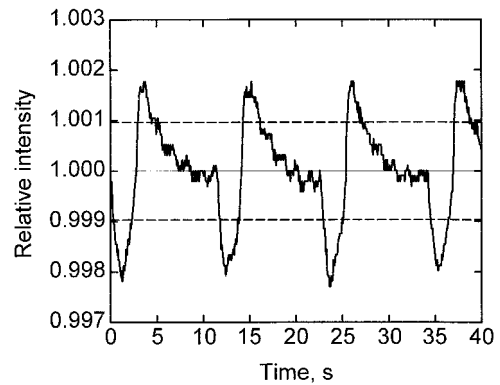


Fig. 3. Measurement of the laser and detector stability. The mean intensity was normalized to 1. The standard deviation of the measured intensity is shown by the dashed lines.

fiber axis had an irradiance distribution that was effectively that of a point source. The cone of light from the PM fiber was collimated with a best-form lens to minimize spherical aberration. The beam was collimated by the critical angle method that is described in Appendix A. The collimated beam was modulated at 500 Hz by a mechanical chopper. An infinity-corrected objective with a numerical aperture of $\text{NA}_{\text{obj}} = 0.65$ was mounted on a z-axis stage. The axis of the collimated beam was aligned coaxially with the axis of the objective.

The fiber mount consisted of a liquid cell with a No. 2 coverslip as the bottom window [see Fig. 4(a)]. The cell was capped by a flame-polished aspheric condensing lens. A hole was drilled through the lens and was concentric to its axis. The outer diameter of a

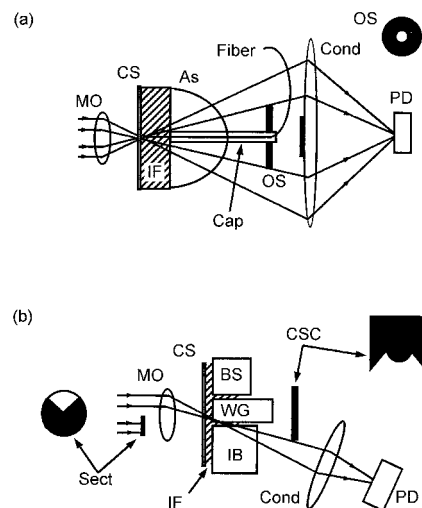


Fig. 4. (a) Schematic of the fiber mount. The components are the microscope objective (MO); coverslip (CS); index-matching fluid (IF); aspheric lens (As); capillary tube (Cap); opaque stop (OS); fiber, condensing lens (Cond); and photodiode (PD). (b) Schematic of the waveguide mount. The components are the sectorial stop (Sect), microscope objective (MO), coverslip (CS), index-matching fluid (IF), back support (BS), waveguide (WG), index-matching block (IB), combined sectorial-circular stop (CSC), condensing lens (Cond), and photodetector (PD).

125- μm capillary tube was turned down to fit into this hole. The capillary was wrapped with Teflon tape to seal it tightly to the lens. Fiber specimens were stripped of their coating, threaded through the capillary tube, cleaned, and then cleaved. The fiber and capillary were passed through the hole in an annular stop and into the cell through the hole in the lens. We focused the refracted light onto a p-i-n photodiode with a 1-cm diameter using the aspheric lens and an additional condensing lens. The center of the condensing lens was covered by black tape to block the light that passed by the hole through the annular stop.

The power of the refracted beam was measured independently of the phase with a digital lock-in amplifier in (R, θ) mode. Use of the digital lock-in amplifier in this way improves the resolution of the measurement because it measures the modulation amplitude independently of the phase. In contrast, a lock-in amplifier that measures only one component of modulation amplitude may have errors owing to phase changes that result from scanning parallel to the direction of rotation of the chopper.

The waveguide mount differed from the fiber mount: It rested on a horizontal platform with a hole drilled through it and did not use the aspheric lens. The hole was coaxial with a silicone rubber O ring. A 22 mm \times 40 mm coverslip was placed on top of the O ring. The back support for the specimen was a 9-mm-thick, 5-cm-diameter fused-silica window that had been cut in half [see Fig. 4(b)]. The endface of the waveguide was placed against the coverslip, and the flat surface of the fused-silica window was pressed against the back surface of the substrate on which the waveguide was manufactured. The surface that contained the waveguides was contacted to an index-matching block, which had approximately the same index of refraction as the substrate. (For a silica waveguide, it was the other half of the fused-silica window; otherwise, it was a polished block of substrate material.) An index-matching fluid optically coupled the block, the coverslip, and the waveguide. The light was collected off axis with the same condensing lens as for the fiber setup, but the condensing lens was oriented at an angle to accommodate only a portion of the refracted beam.⁸

The z -axis stage was positioned by a stepping motor capable of 0.1- μm steps. At 635 nm, Shillaber's equation [Eq. (8)] gives 0.6 μm for the depth of focus. Hence the step was small enough for accurately locating the focal plane at the endface of the specimen.

The fiber and waveguide mounts were designed to be interchangeable and fit into a mount that allowed tilting the specimen so that it lay normal to the axis of the beam. This mount was fixed to (x, y) scanning stages, both of which had steps of 0.1 μm .

We aligned our specimen by directing the backreflections from all components into the PM fiber. This requirement ensured precise angular alignment of the specimen endface and the beam axis throughout the system. Before a measurement, a neutral

density filter was placed against the best-form lens between the lens and the fiber output to prevent the backreflections from destabilizing the laser. We estimate that the filter diminished the intensity of all individually focused backreflections at the output of the patchcord to approximately 4×10^{-6} or less of the output power of the laser. The wedge in the filter was apparently not a problem, inasmuch as the final focusing and positioning of the specimen were carried out with the filter in place.

Light was focused onto the endface of the specimen through the coverslip. The light that exited the fibers and waveguides consisted of refracted light, leaky mode light, and guided light. The leaky mode light and the guided light were blocked by a stop, which was an annulus for fiber specimens and a combined sectorial-circular stop for the waveguides (see Fig. 4). The circular stops were positioned to block a numerical aperture of approximately 0.7 NA_{obj} to ensure diffraction-limited spatial resolution.

The sectorial stop [Sect in Fig. 4(b)] that precedes the objective subtends an angle of approximately 90°. For 2-D scans, it is important that this stop be the limiting aperture of the system. That is, the sector that follows the waveguide is merely a glare stop and must transmit all the light that emerges from the block (IB) at an angle greater than the angle subtended by the circular stop. If this condition is not satisfied, then the waveguide will cast a shadow that appears as a winglike artifact in the index profile. Similarly, the beam that emerges from the block is highly aberrated and cannot be focused to a small point. We therefore used a large-area detector to ensure that all the transmitted light falls onto the detector. Because there is no dearth of power, we could have used an integrating sphere and a smaller detector instead.

The maximum sampling rate for the system during each linear scan was approximately 10–15 Hz. The main factor limiting the acquisition speed was the requirement to wait until the stepping motors had stopped moving followed by a period of five time constants of the lock-in amplifier, or 50 ms.

4. Experiment and Discussion

A. Measuring the Stability of the Laser and Detector

Figure 3 shows a typical intensity resolution measurement for the profiler. Refracted light intensity data were accumulated for 10,000 s at intervals of 61 ms. The intensity fluctuations of the source are both periodic and, on a smaller scale, random. The periodic variations occurred approximately every 11 s. So far we have made no attempt to eliminate them, as for example, by using a reference detector. We determined from the intensity measurement a maximum relative deviation of 0.22% and a relative standard deviation of 0.1% for the intensity. Once the index of refraction has been calibrated to the measured intensity, the peak-to-peak deviation and the standard deviation of the index can be computed. After system warmup, a

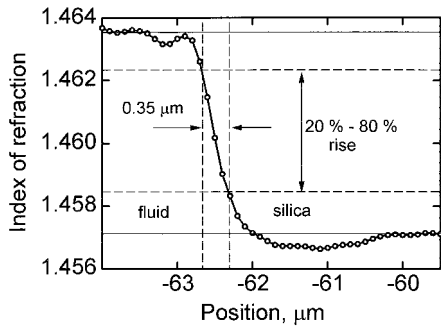


Fig. 5. Refracted-ray scan across the interface between a silica fiber and the index-matching fluid. The 20–80% rise is approximately 35 μm .

specific configuration of the lock-in amplifier and the optics will typically have the same intensity fluctuations on any given day. However, the fluctuations and therefore the resolution can change form and magnitude over long times or with changes in the configuration of the system.

B. Fiber Index Profiles

Before we collected the data, we focused the beam onto the endface of the specimen by repeatedly scanning over the index step between the fiber cladding

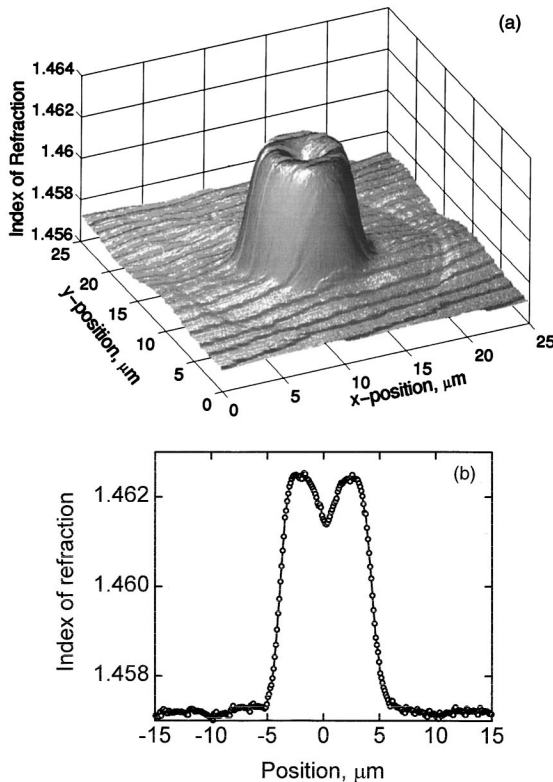


Fig. 6. (a) 2-D index profile of a single-mode fiber. A small, annular index depression between the inner and the outer cladding regions is visible. The annulus is 0.7 μm wide and has a radius of 10.6 μm . The diagonal lines are due to aliasing of the scan period with periodic fluctuations in the laser. (b) 1-D index profile obtained from a cross section of the 2-D index profile shown in (a).

and the index-matching oil. We found the best focus by maximizing the slope of the measured intensity versus position across the step. When the system was configured for fibers, the slope decreased noticeably when the objective was approximately 0.5–0.6 μm out of focus. This depth of focus is consistent with Shillaber's equation [Eq. (8)]. Spatial resolution, measured as the 20–80% rise, was sensitive to as little defocusing as 0.3 μm . When the objective was optimally focused, the 20–80% rise was 0.35 μm (see Fig. 5). For comparison, in a diffraction-limited system with coherent light, the 20–80% rise equals approximately one half of the Rayleigh limit or, in our case, approximately 0.3 μm . The system is therefore diffraction limited or nearly so.

We measured the 2-D index profile of a single-mode fiber produced by the telecommunications industry in the early 1990's [Fig. 6(a)]. Consisting of 250,000 data points, the scan covered an area of 50 $\mu\text{m} \times 50 \mu\text{m}$ and took overnight to complete. Only the central quarter of the total scan is shown in Fig. 6(a). We monitored the air temperature with a sensor that sat atop the cell during the experiment; it was stable within 0.6 K during the scan. The index of the index-matching fluid had a temperature coefficient of $-3.9 \times 10^{-4}/\text{K}$. Figure 6(b) shows a one-dimensional (1-D) cross section through the axis of the fiber.

The 11-s period of the intensity fluctuations of the source was aliased with the period of each linear scan, which caused the diagonal lines in Fig. 6(a). The maximum deviation of 0.22% of the periodic power fluctuations of the laser intensity represents approximately 1.9% of the difference in refracted light intensity measured between the core and the cladding. Because the core-cladding index difference was $\Delta n = 0.0052$, the maximum systematic fluctuation of the measured index of refraction was approximately 1×10^{-4} . However, because the eye can discriminate against regular patterns to infer an underlying feature, index structures with large spatial scale were plainly observable with a resolution finer than the maximum fluctuation.

If we use the relative standard deviation of the laser power (0.1%) as the measure of the discernible resolution of this scan, then the resolution to which we can resolve index features in Fig. 6 is approximately $0.1\%/0.22\% \times 1 \times 10^{-4} = 4 \times 10^{-5}$. Thus, even though we are using an index-matching fluid whose index of refraction has a fairly high uncertainty, our 2-D profiler can resolve index features with a resolution that is approximately 14 times smaller than the standard uncertainty of the index measurement (which is approximately 6×10^{-4}). Furthermore, this resolution is a factor of 5 finer than the uncertainty that can be obtained with standard reference materials. The ability to resolve detail in the measurement (the resolution) is independent of the uncertainty of the indices of the reference points.

The high resolution in the measurement made it possible to resolve in the cladding an annular index

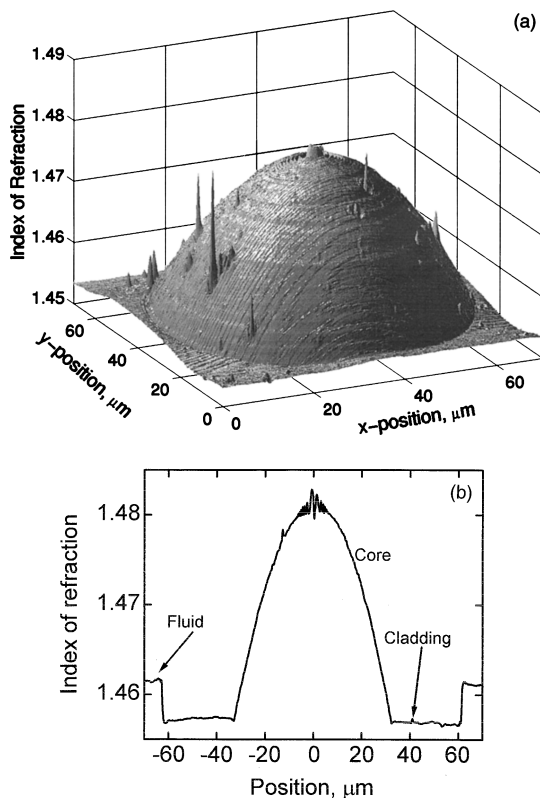


Fig. 7. (a) 2-D index profile of a multimode fiber. (b) 1-D index profile obtained from a cross section of the 2-D index profile shown in (a).

depression, which had a width of approximately $0.7 \mu\text{m}$ and a radius of approximately $10.6 \mu\text{m}$. This index depression is barely resolved but appeared to have a depth of 1×10^{-4} . We discussed the depression with a representative of the manufacturer and concluded that it was caused by a strained layer or a layer of lower density, which was formed at the boundary where the inner cladding and the outer cladding were fused together in the preform.

Figure 7 shows the index profile of a multimode fiber. The 2-D scan spans $70 \mu\text{m} \times 70 \mu\text{m}$ and consists of 490,000 data points. The concentric rings in Fig. 7(a) disclose that the deposition layers in the fiber preform did not coalesce completely to a smooth index profile when the preform was collapsed and when the fiber was drawn. The large oscillations near the axis, seen in Fig. 7(b), have been noted before. However, the smaller index oscillations at larger radii from the axis have not been resolvable until now, as far as we know. The index variations at large radii are observable in Fig. 7(a) only because the 2-D plot allows the eye to integrate over a large number of data points and infer the oscillations. The 1-D index profile does not allow such integration, so the index variations are not detectable at large radii. Much qualitative information can therefore be gleaned from a 2-D scan. The spikes in Fig. 7(a) result from contaminants or defects on the fiber end-face.

C. Index Profiles of Planar Waveguides

To test the planar-waveguide configuration, we first constructed a simple miniature cell by using two, $\sim 1\text{-cm}$ -long pieces of fiber stripped of their coating and clamping them between the two blocks. The index-matching fluid was held in place between the fibers and the blocks by capillary action. A fiber specimen was placed in the center of this miniature cell.

We tested the spatial resolution for 2-D profiling of waveguides using a different piece of the single-mode fiber that had been used for fiber scanning (Fig. 8). The 20–80% rise across the edge between the fluid and the fiber cladding was approximately $0.6\text{--}0.7 \mu\text{m}$, or twice the value in the fiber configuration [see Fig. 8(b)]. The 2-D scan resolves the index dip in the center and shows slight evidence of the annular index dip at a radius of $10.6 \mu\text{m}$. The spatial resolution of the data obtained with the waveguide configuration was approximately the same as the width of the annular index dip, so that dip is less clearly resolved in Fig. 8(a) than in Fig. 6(a).

We think that the poorer spatial resolution occurs primarily because the sector diminishes the numerical aperture of the light that is focused onto the specimen. The depth of focus in the waveguide configuration was approximately $2 \mu\text{m}$, which is greater than in the fiber configuration and is consistent with the larger resolution limit.

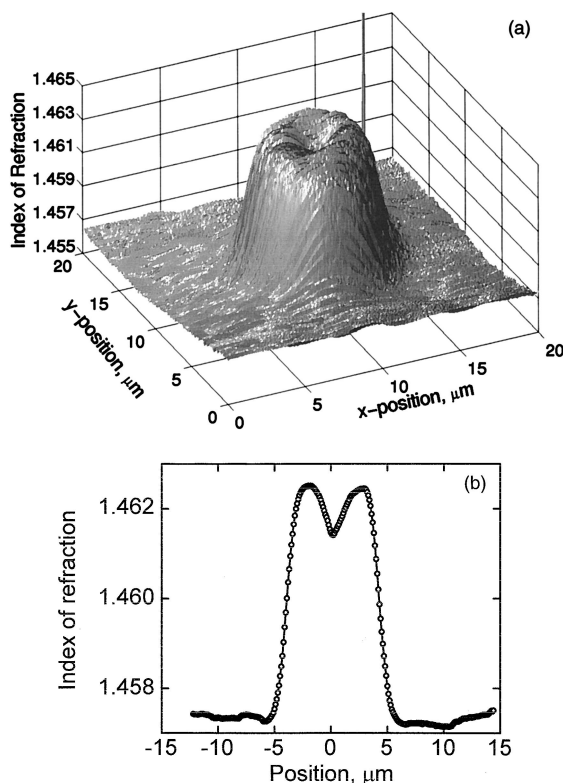


Fig. 8. (a) 2-D index profile of the same single-mode fiber as in Fig. 3, but made using waveguide mount and the sector. (b) 1-D index profile obtained from a cross section of the 2-D index profile shown in (a).

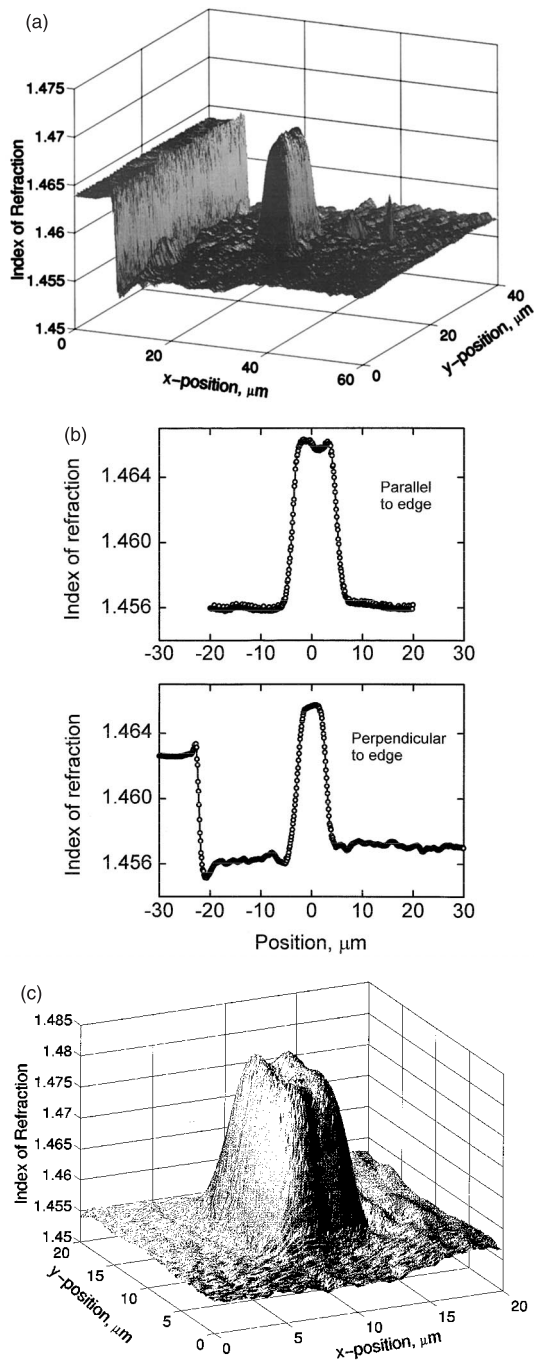


Fig. 9. (a) 2-D index profile of a buried waveguide. (b) 1-D index profiles, transverse and parallel to the surface of the substrate, obtained from a cross section of the 2-D index profile shown in (a). (c) 2-D index profile of another waveguide from the same substrate as Fig. 9(a), courtesy of Eric Jacobsen, Professional Research Experience Program Fellow at the National Institute of Standards and Technology (NIST). Waveguides courtesy of Richard Maschmeyer, Corning, Inc.

Figure 9 is a refracted-ray scan of a buried waveguide on a silica substrate. The left wall in Fig. 9(a) is the boundary between the specimen and the index-matching fluid. The rectangular structure of the guide is clearly discernible at the boundary be-

tween the underlayer and the overlayer. The underlayer and the overlayer have different indices of refraction, as we can see from Fig. 9(b). Finally, Fig. 9(c) is a closeup of another waveguide on the same substrate; it displays an index dip of unknown etiology and is parallel to the surface of the substrate.

For these specimens, we did not see the effect of aliasing the laser with the raster period. We did, however, observe the aliasing when scanning in the region that contained the fluid. The specimen was cleaned and remounted several times, but the index scans failed to display the aliasing. We conclude from this evidence that we cannot see the aliasing lines anywhere on the endface of the waveguide because either (1) the specimen is optically inhomogeneous at a level that exceeds the maximum deviation of the resolution of 1×10^{-4} or (2) there are polishing scratches on the endface. If there are large inhomogeneities, then it is likely that they may be pronounced enough to scatter significant power anywhere along the waveguide. If there are scratches on the endface, they could affect the coupling of light into and out of the guide. In either case, these imperfections will be of concern to the manufacturer.

We also profiled a surface waveguide that had been used as the lasing medium in an external cavity configuration. The waveguide was pumped by 979-nm radiation and lased at wavelengths in the vicinity of 1540 nm. The substrate was a phosphate glass that had been codoped with 1.15% Er_2O_3 (0.99×10^{20} ions/cm³) and 4.73% Yb_2O_3 (3.97×10^{20} ions/cm³), by mass. The guiding channel was created by thermal exchange of K^+ ions from a KNO_3 melt with Na^+ ions in the phosphate glass. The ions were exchanged for 4 h through a 0.2- μm -thick, 6.5- μm -wide Al aperture at a temperature of 375 °C.⁹

The index of the immersion fluid was made nearly equal to the index of the substrate to create good contrast for resolving the index step at the surface of the guide. The 20–80% rise is approximately 0.6 μm wide, indicating nearly diffraction-limited spatial resolution for this measurement.

Figure 10 is a topographic map of this waveguide and reveals that the exposed surface of the waveguide under the mask is recessed by 1–2 μm because of the ion exchange. The mechanism that causes the recession is currently under investigation; most probably it is collapse owing to stress, not to etching, because the recession does not appear until the mask is removed. The relatively sharp corners also suggest stress rather than etching. Additionally, the map reveals that the region of highest index (red) is located somewhat below the surface of the substrate. Finally, it reveals a scratch that appears (falsely) as a linear index depression that runs across the profile in the region between $x = 45 \mu\text{m}$ and $x = 60 \mu\text{m}$. Figure 11 is a cross section of the same waveguide perpendicular to the surface of the substrate.

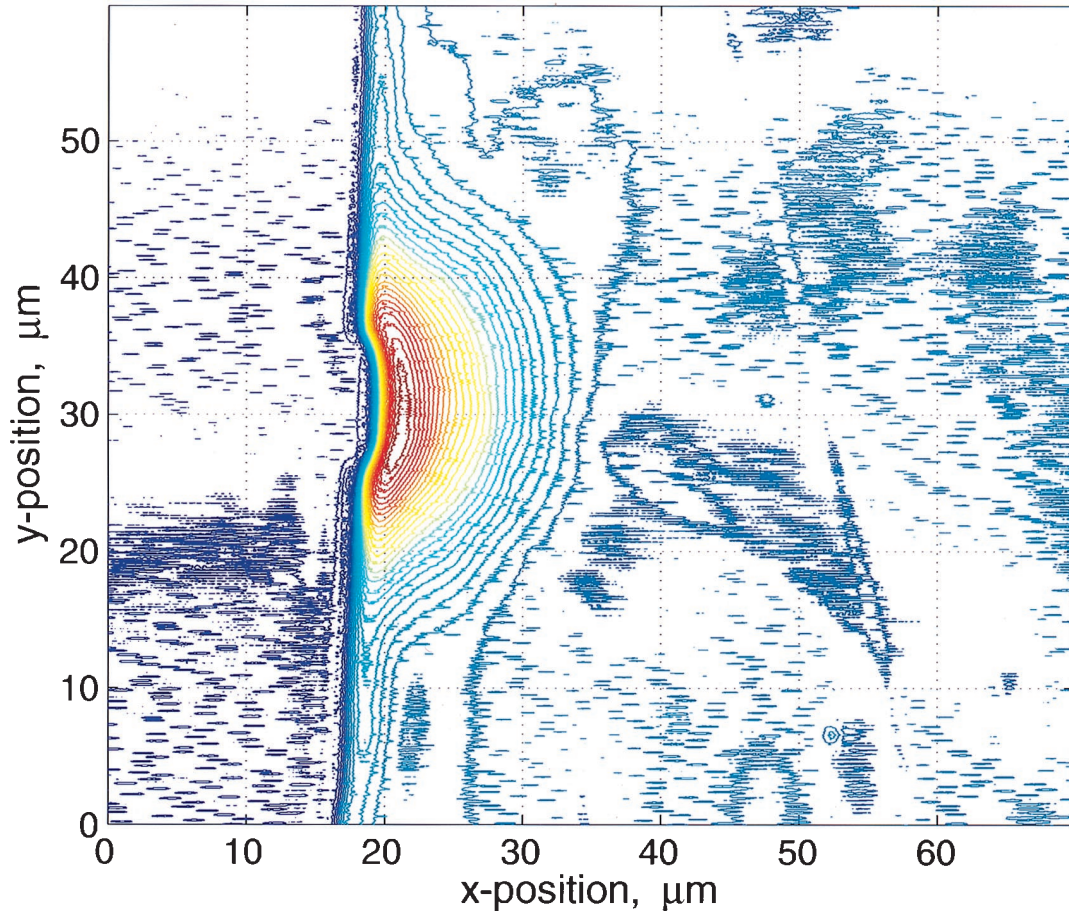


Fig. 10. Topographic map of a thermally diffused surface waveguide.

5. Conclusions

We make an important distinction between the uncertainty and the resolution of the index profile measured by refracted-ray scanning. Although the uncertainty is limited by the uncertainties in the reference materials to the order of a few parts in 10^{-4} , the resolution is 4.3×10^{-5} and is limited by the stability of the source and the detector and the homogeneity of the optical media such as the coverslip. The resolution of the index profile can be improved by

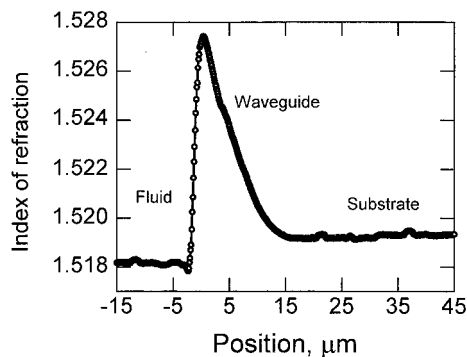


Fig. 11. 1-D index profile, transverse to the top surface of the guiding channel, of the index profile shown in Fig. 10. Waveguide courtesy of David Funk, NIST Postdoctoral Fellow.

making improvements to the stability of the apparatus, whereas the uncertainty can be improved by better knowledge of the indices of the optical materials in the cell.

Additionally, 2-D scanning can provide important qualitative information for evaluating fibers and planar waveguides. This is in addition to the usual role of refracted-ray scanning in quantitative index profiling. In our system we measured an index depression of 1×10^{-4} between the inner and outer silica claddings of a single-mode fiber. We have also shown that the index profile of a multimode fiber did not coalesce to a smooth profile. We have used refracted-ray scanning to reveal scratches or index inhomogeneities on the endface of buried and surface waveguides, and we used a topographic map to show that the surface of a waveguide had become recessed during the waveguide's manufacture.

Appendix A: Critical Angle Method for Beam Collimation

When a collimated beam strikes an interface at an angle slightly less than the critical angle, the transmitted beam will form a thin line on a far wall. This thin line occurs because all the rays across the wave front of a collimated beam are parallel and will map to the same refraction angle of nearly 90° . The re-

fracted beam can be observed near the critical angle of incidence while the collimating lens is translated until the sharpest line is observed. When the beam is not collimated, the refracted line will display a pincushion for a converging beam and a barrel effect for a diverging beam.

Special thanks to John Baines of the National Physical Laboratory in the United Kingdom for his critical reading of the manuscript; to Eric Jacobsen for his help with the 2-D figures; to Richard Maschmeyer of Corning, Inc. for providing the silica waveguide and David Funk of the National Institute of Standards and Technology (NIST) for providing the phosphate glass waveguide; and to Katherine Pagaoga of NIST for translating the manuscript from one format to another, dissimilar format.

References and Notes

1. M. Young, "Optical fiber index profiles by the refracted-ray method (refracted near-field scanning)," *Appl. Opt.* **20**, 3415–3421 (1981).
2. K. L. White, "Practical application of the refracted near-field technique for the measurement of optical fiber refractive index profiles," *Opt. Quantum Electron.* **11**, 185–196 (1979).
3. Anonymous, "Refractive index profile, refracted-ray method," Fiber optic Test Procedure FOTP-44b, TIA/EIA-455-44b (Telecommunications Industry Association, 2500 Wilson Blvd., Suite 300, Arlington, Va. 22201-3384, 1992). Here we adopt the TIA's preferred term, refracted-ray method, instead of refracted near-field scanning, in part because currently near-field scanning can reasonably be assumed to mean optical probe microscopy.
4. J. W. Fleming, "Material and mode dispersion in $\text{GeO}_2 \cdot \text{B}_2\text{O}_3 \cdot \text{SiO}_2$ glasses," *Amer. Ceram. Soc. Bull.* **59**, 503–507 (1976).
5. K. W. Raine, J. G. N. Baines, and D. E. Putland, "Refractive index profiling—state of the art," *J. Lightwave Technol.* **7**, 1162–1169 (1989).
6. *Specialty Optical Liquids* (R. P. Cargille Laboratories, Cedar Grove, N.J., undated).
7. J. Delly, *Photography Through the Microscope*, 9th ed. (Eastman Kodak Company, Rochester, N.Y., 1988).
8. R. Göring and M. Rothhardt, "Application of the refracted near-field technique to multimode planar and channel waveguides in glass," *J. Opt. Commun.* **7**, 82–85 (1986); N. Gisin, J. P. Pelloux, P. Stamp, N. Hori, and M. Masuyama, "Alternative configuration for refracted near-field measurements of index of refraction on glass-integrated-optics waveguides," *Appl. Opt.* **31**, 7108–7112 (1992).
9. D. S. Funk, D. L. Veasey, P. M. Peters, N. A. Sanford, N. H. Fontaine, and M. Young, "Erbium/ytterbium-co-doped glass waveguide laser producing 170 mW of output power at 1540 nm," *Conf. Digest, Optical Fiber Conf.*, 1999; D. L. Veasey, D. S. Funk, P. M. Peters, N. A. Sanford, G. E. Obarsky, N. H. Fontaine, M. Young, A. P. Peskin, W.-C. Liu, S. N. Houde-Walter, and J. S. Hayden, "Yb/Er-codoped and Yb-doped waveguide lasers in phosphate glass," *J. Non-Cryst. Solids* (to be published).